Journal of Intelligent Systems and Control
https://www.acadlore.com/journals/JISC

Control of DMC-Based LLC Resonant Converters

Xixi Han*, Zhibo Lin, Keqi Kang, Xiaopei Zhu

School of Electronic and Information Engineering, Zhongyuan University of Technology, 451191 Zhengzhou, China

* Correspondence: Xixi Han (6580@zut.edu.cn)

Received: 10-10-2023 **Revised:** 11-16-2023 **Accepted:** 11-28-2023

Citation: X. X. Han, Z. B. Lin, K. Q. Kang, and X. P. Zhu, "Control of DMC-based LLC resonant converters," *J. Intell Syst. Control*, vol. 2, no. 4, pp. 209–219, 2023. https://doi.org/10.56578/jisc020403.

Abstract: LLC resonant converters own high power efficiency and density, and are widely used in electric vehicles, intelligent and communication power sources, and other fields. The converters cannot obtain accurate mathematical models and their nonlinear characteristics are complex. Therefore, traditional proportional-integral (PI) control cannot achieve control effect well. The dynamic matrix control (DMC) strategy was applied to the converter model, aiming to improve the system's dynamic response and reduce overshoot. In addition, the DMC algorithm was used in this study to achieve precise system control. The algorithm is robust, and can improve the system's stability and reliability. At the same time, the system can be flexibly controlled through parameter adjustment. Furthermore, a voltage prediction closed-loop controller was designed to enhance the system's dynamic performance. In addition, a simulation model was built based on this to verify the feasibility and effectiveness of the scheme. The simulation results showed that the DMC algorithm suppressed overshoot and improved dynamic response effectively.

Keywords: Dynamic matrix control; LLC resonant converter; Voltage prediction closed-loop controller; Dynamic performance; Rolling optimization

1 Introduction

With the development of new energy technology, vehicles with more types, led by electric vehicles, have emerged in the automotive market. Electric vehicles have been recognized as the future development trend of the automotive industry [1, 2]. For their applications, it is essential to construct charging stations. As an important component of the internal circuit of charging stations, the study of direct current/direct current (DC/DC) converters has attracted significant scholarly attention globally. As a type of DC/DC converter, the full-bridge LLC resonant converter utilizes resonant circuits to achieve soft switching technology [3], which enables zero-voltage switching (ZVS) at the primary side switch and zero-current switching (ZCS) at the secondary side rectifier diodes. Soft switching technology helps reduce switching losses and improve power efficiency, compared to hard switching. Furthermore, the converter has reduced voltage stress for switching devices and heightened transformer utilization efficiency. Therefore, the converter has higher energy conversion efficiency and power density. At the same time, the circuit has smaller electromagnetic interference and stronger electromagnetic compatibility ability [4–6]. The converter's advantages enable it to be widely used in communication and aviation power supplies, power adapters, energy routers and other fields [7, 8].

The LLC resonant converter, recognized as a complex, non-linear system, employs frequency control to modulate its resonant impedance, thereby achieving desired output levels [9, 10]. Research into control methods for LLC resonant converters has revealed that systems using traditional PI control display a slow dynamic response, especially under substantial load fluctuations. Fang et al. [11] devised a variable domain fuzzy neural PI intelligent controller by integrating fuzzy control, neural network control, and variable domain principles, enhancing control performance but increasing both design complexity and computational load. Kang and Cho [12] introduced a dual closed-loop feedback control strategy featuring a current inner loop fuzzy self-tuning PI regulator, which improved control performance through enhanced current inner loop control, albeit complicating circuit design due to additional circuit sampling requirements. Pandey and Singh [13] implemented a strategy combining variable frequency control with phase shift control, effectively addressing voltage gain distortion issues in light load conditions but resulting in slow system dynamic response and substantial overshoot.

The traditional PI control has simple structure and is capable of steady-state error-free operation. However, unchanged parameters and modes are adopted for handling dynamic processes with multiple variables. Therefore, there is a certain contradiction between balancing stability, responsiveness, and accuracy. The DMC algorithm is an advanced optimization algorithm applied to control systems. Its implementation is based on matrix and control theory, and precise control of the system is achieved by adjusting matrix parameters. The algorithm has the advantages of accuracy, robustness, and adaptability, and is widely used in industrial automation control, power system control, robot control, and traffic control. This study applies the DMC algorithm to the LLC resonant converter model, designing a voltage prediction controller for closed-loop control of the LLC resonant converter. Rolling optimization algorithm and feedback correction are utilized to achieve tracking control of the output voltage. This method has the characteristics of simple algorithm and small real-time calculation, and has certain application value. By building a simulation model, the feasibility and effectiveness of the algorithm were verified. A comparative analysis of DMC predictive control and PI control revealed the superior performance of the former.

2 Methodology

2.1 Topology of the LLC Resonant Converter

The circuit topology of the full-bridge LLC resonant converter is illustrated in Figure 1. This configuration encompasses an input DC source V_{in} and an output DC voltage U_o. Integral to the circuit's initial segment are the primary side switch S_1-S_4, its anti-parallel diode D_1-D_4, and parasitic capacitor C_1-C_4. Central to the operation are the resonant capacitor C_r and inductor L_r, through which the resonant current I_{Lr} flows. The high-frequency isolation transformer T, characterized by a specific transformer ratio n : 1, along with its excitation inductance L_m that carries the excitation current I_{Lm}, are also crucial components. On the secondary side, high-frequency rectifying diodes D_1-D_4, an output filter capacitor C_0, and an output load resistor R are featured.

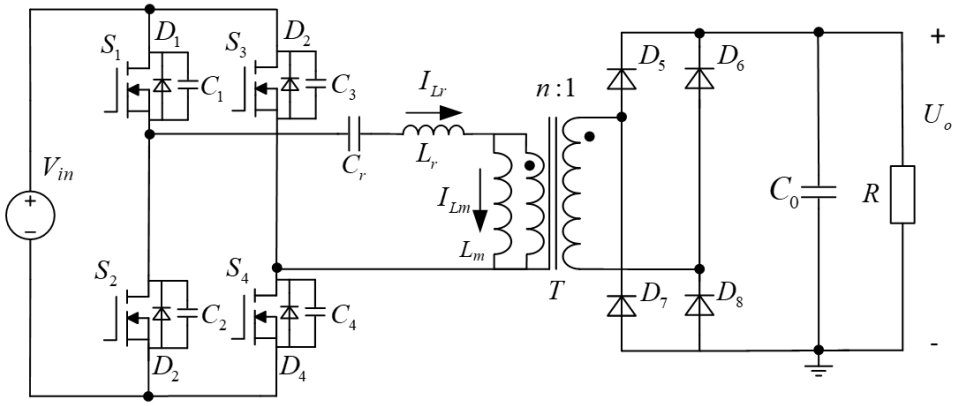

Figure 1. Circuit topology of the full-bridge LLC resonant converter

During operation, the LLC resonant converter exhibits two resonant frequencies, determined by the involvement of the transformer's excitation inductance in resonance. These frequencies are identified as the series resonant frequency f_r and the series-parallel resonant frequency f_{r1}, respectively formulated in Eqs. (1) and (2). Depending on the relationship between the switching frequency f_s and these resonant frequencies, the converter's operating frequency is categorized into three distinct scenarios, namely, $f_s > f_r$, f_s=f_r, and $f_{r1} < f_s < f_r$.

$$f_{r1} = \frac{1}{2\pi\sqrt{L_r C_r}} \tag{1}$$

$$f_{r1} = \frac{1}{2\pi\sqrt{(L_\mathrm{r} + L_\mathrm{m})\, C_r}} \tag{2}$$

The resonant network, comprising resonant capacitor C_r, inductor L_r, and excitation inductance L_m, forms the primary characteristic of the LLC resonant converter [14, 15]. The fundamental wave analysis method is used to establish a mathematical model. The model delineates the relationship between the DC voltage gain M and the normalized switching frequency f_n, as expressed in Eq. (3).

$$\begin{cases} M = \dfrac{1}{\sqrt{\left(1+\frac{1}{\lambda}\left(1-\frac{1}{f_n^2}\right)\right)^2+\left(f_n-\frac{1}{f_n}\right)^2 Q^2}} \\ Q = \dfrac{\pi^2 R_L}{8n^2}\sqrt{\dfrac{L_r}{C_r}} \\ \lambda = \dfrac{L_m}{L_r} \\ f_n = \dfrac{f_s}{f_r} \end{cases} \tag{3}$$

where, the circuit's quality factor Q, the ratio λ of excitation inductance to resonant inductance, and the normalized switching frequency f_n are pivotal factors.

When maintaining a constant inductance ratio λ, the DC voltage gain's variation M with normalized frequency, denoted as f_n, under varying values of the quality factor, denoted as Q, is depicted in Figure 2. Three operational regions are distinguishable in this curve. The converter operates in an inductive state in buck mode in Region 1, where the primary side switch achieves ZVS, but the secondary side rectifying diodes experience hard switching, leading to reverse recovery losses. Region 2 sees the converter operating in an inductive state in boost mode, enabling ZVS for the primary side switch and ZCS for the secondary side rectifying diodes. Region 3, wherein the converter operates in a capacitive state, is characterized by the primary side switch achieving ZCS but not ZVS, necessitating avoidance of this operational area. Consequently, parameter design focuses on ensuring the converter operates in regions conducive to ZVS, specifically, Regions 1 and 2.

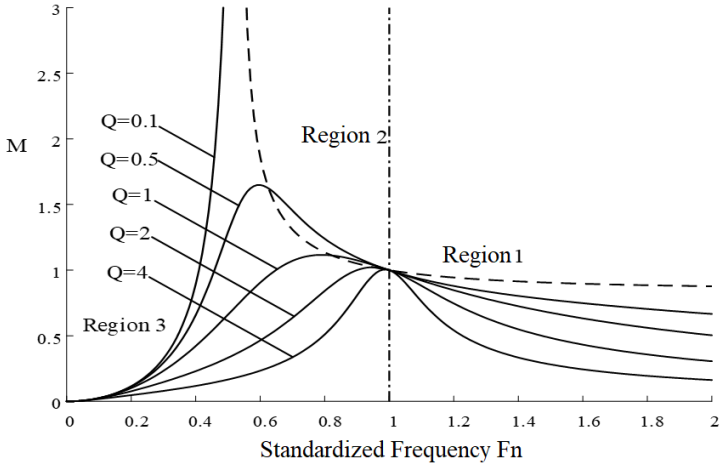

Figure 2. Voltage gain variation curve

2.2 Control Principle of the LLC Resonant Converter

The relationship between the voltage gain of the LLC resonant converter and its switching frequency is a key focus in controlling its output voltage. Pulse Frequency Modulation (PFM) is utilized for varying frequency, thereby regulating the output voltage of the full-bridge LLC resonant converter. For modeling the LLC resonant converter, a small-signal model analysis method is employed, leading to the design of a voltage closed-loop controller. The configuration of a conventional PI control system is depicted in Figure 3, where the voltage feedback module gathers the output voltage value for comparison with the preset value at the input stage. The voltage-to-frequency conversion module converts the voltage control output from the PI controller into a frequency value, which the PFM module subsequently transforms into a corresponding square wave control signal.

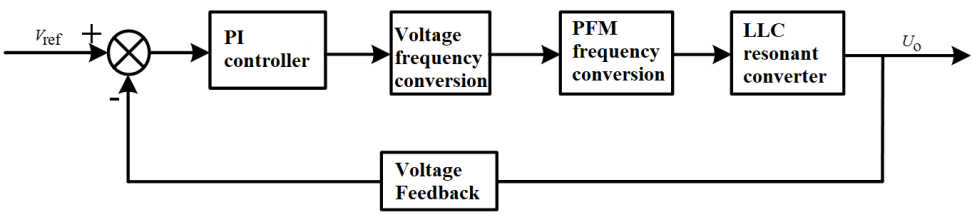

Figure 3. Configuration of the PI control system

Disregarding the effects of circuit harmonics, the small-signal transfer function relating the frequency of the LLC resonant converter to its output voltage [16, 17] is represented as:

$$G_{vs} = \frac{A_{vf}}{\left(1 + \frac{S}{\omega_p}\right)\left(1 + \frac{S}{Q\omega_o} + \frac{S^2}{\omega_o^2}\right)} \tag{4}$$

where, A_{vf} denotes the open-loop low-frequency gain, and $-\omega_p$ symbolizes the low-frequency pole, associated with resonant parameters ω_o. The expression for the low-frequency gain A_{vf} is:

$$A_{vf} = \frac{\frac{2V_{in}}{\lambda f_{r1} f_n^3}\left(1 + \frac{1}{\lambda} - \frac{1}{\lambda f_n^2}\right) + Q^2\left(f_n - \frac{1}{f_n}\right)\left(1 + \frac{1}{f_n^2}\right)}{\left[\left(1 + \frac{1}{\lambda} - \frac{1}{\lambda f_n^2}\right)^2 + Q^2\left(f_n - \frac{1}{f_n}\right)^2\right]^{\frac{3}{2}}} \tag{5}$$

Applying a PI control strategy for the controller design of the LLC resonant converter, the transfer function of the PI controller is outlined as:

$$G_c = K_p + \frac{K_i}{s} \tag{6}$$

where, K_p symbolizes the proportional coefficient, and K_i denotes the integral time constant. These parameters are deduced based on the system model. Figure 4 illustrates the system diagram of traditional PI control, with K_{vf} representing the coefficient of the voltage-to-frequency conversion module, $G_{vs}(s)$ being the transfer function of the converter within the system, and $H(s)$ serving as the transfer function for voltage feedback in the system's control loop.

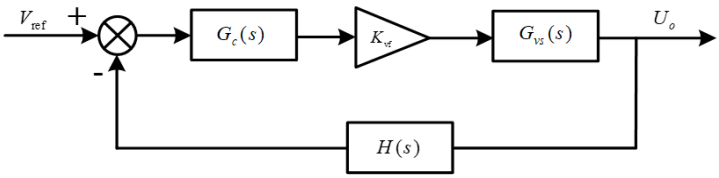

Figure 4. System diagram of traditional PI control

2.3 Investigation of the DMC Strategy

DMC, a predictive control algorithm, was initially proposed in 1980 by researchers including Cutler. This methodology relies on the collection of step response data from the model, rather than the model's specific form, to establish a predictive model [18–20]. DMC is renowned for its rapid response to system changes and notable robustness [21, 22].

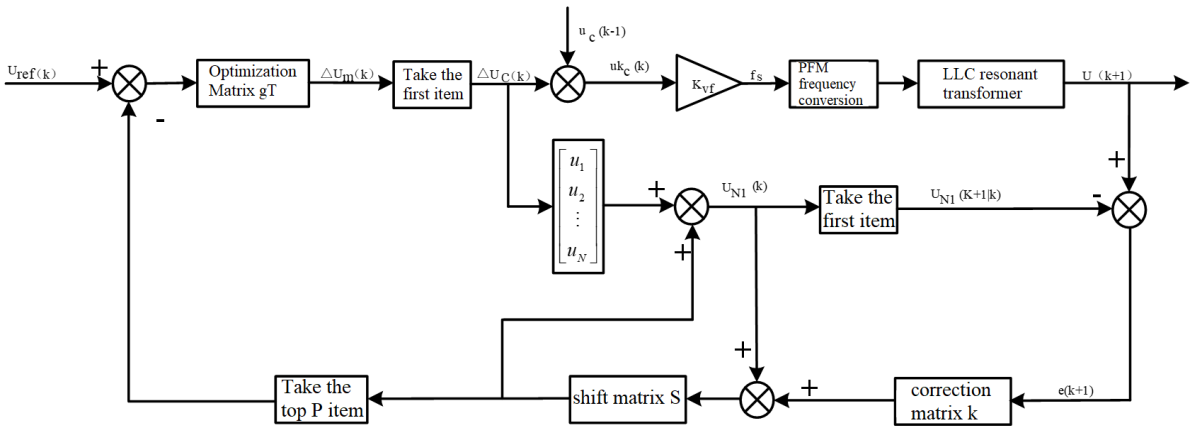

Figure 5. DMC predictive model for LLC resonant converter

In this research, the proposed DMC predictive model for the LLC resonant converter is demonstrated in Figure 5. The DMC strategy is adopted to supplant the traditional PI control strategy, effectively addressing the issues of sluggish dynamic response and pronounced overshoot in the system. In this process, the differences between the vector of predetermined voltage values and the initial predicted voltage values for the initial P terms are calculated. This differential is applied to the optimization model, which then computes the control increments for the subsequent P moments. Furthermore, using the predictive model, the predicted voltage output values for the future N moments are derived. The primary element of the control increment is transformed into a frequency value, subsequently applied to the LLC resonant converter using a PFM module. A comparison between the actual output voltage value and the initial value of the voltage prediction is conducted, with the subsequent feedback correction yielding a revised initial voltage prediction value.

2.3.1 Predictive model

The formulation of a predictive model for the LLC resonant converter commences with the sampling of the unit step response of the output voltage U_o. Under a constant input voltage, and with the switching frequency f_s aligned with the resonant frequency f_r, the sampled output voltage (U_o) values of the LLC resonant converter's step response are acquired. These values, denoted as $u_i = x(iT)$, with $i = 1, 2, \cdots, N$, where T symbolizes the sampling period and N signifies the modeling time domain, vectors $u = \begin{bmatrix} u_1 & u_2 & \cdots & u_N \end{bmatrix}$ collectively form the system's model vector. It is crucial that the final value u_N in this sequence closely approximates the steady-state value of the system's step response.

Owing to the proportionality and superposition characteristics inherent in linear systems, the output values for voltage prediction are deduced from the predictive model. Starting from the k-th moment, a cumulative addition of M control increments $\Delta u_c(k)$, $\Delta u_c(k+1)$,$\cdots$,$\Delta u_c(k+M-1)$ is performed to ascertain the predicted output voltage at subsequent $k+P$ moments, as expressed in Eq. (7):

$$U_{PM}(k) = U_{P0}(k) + A\Delta U_M(k) \tag{7}$$

where,

$$U_{PM}(k) = \begin{bmatrix} u_M(k+1|k) & u_M(k+2|k) & ... & u_M(k+P|k) \end{bmatrix}^T$$

$$U_{P0}(k) = \begin{bmatrix} u_0(k+1|k) & u_0(k+2|k) & ... & u_0(k+P|k) \end{bmatrix}^T$$

$$A = \begin{bmatrix} u_1 & & & 0 \\ u_2 & u_1 & & \\ \vdots & \vdots & \ddots & \\ u_M & u_{M-1} & ... & u_1 \\ \vdots & \vdots & \vdots & \vdots \\ u_P & u_{P-1} & ... & u_{P-M+1} \end{bmatrix}$$

$$\Delta U_M(k) = \begin{bmatrix} \Delta u_c(k) & \Delta u_c(k+1) & \cdots & \Delta u_c(k+M-1) \end{bmatrix}^T$$

where, $U_{PM}(k)$ signifies the predicted output voltage at a future moment k, influenced by M control increments at future P moments. $U_{P0}(k)$ represents the initial predicted output voltage at future P moments, under the presumption of unchanged control action from moment k. A symbolizes a Toeplitz matrix, a $P \times M$-dimensional constant matrix constituted by the system's step response coefficients, mirroring the system's dynamic behavior. $\Delta U_M(k)$ is a vector comprising M control increments. P and M correspond to the optimization and control time domains of the model, respectively.

The determination of the modeling time domain, denoted as N, necessitates careful consideration of the sampling period. A value too diminutive might not suffice u_N to mirror the step response's steady-state value, while an excessively large value could impose undue computational burdens, potentially compromising the real-time control efficacy of the system. Typically, this value N is chosen within the range of 20 to 60. The optimization time domain P significantly influences the stability and responsiveness of the control system; an unduly small value may risk system robustness or induce instability, whereas an overly large value might lead to a sluggish dynamic response. The control time domain M is usually set at half the value of the optimization time domain P, with $M \leq P \leq N$, to maintain system stability and robustness without excessively amplifying M.

2.3.2 Rolling optimization

DMC employs an optimal control strategy where the optimization process is continuously advanced over time. The optimization at any given moment focuses on a local objective, predicting output for upcoming moments based on the accumulated M control increments from the current moment. The objective is to ensure that the predicted output values of subsequent P moments align closely with the preset values, while maintaining control increments within limits to prevent abrupt variations. The system utilizes a quadratic performance criterion for this rolling optimization process, which at moment k is defined as:

$$J = \|U_{ref}(k) - U_{PM}(k)\|_Q^2 + \|\Delta u_M(k)\|_R^2 \tag{8}$$

where, $U_{ref}(k)$ is a column vector comprising the trajectory of preset output voltage values.

$$U_{ref}(k) = \begin{bmatrix} u_{ref}(k+1) & u_{ref}(k+2) & \cdots & u_{ref}(k+P) \end{bmatrix}^T$$

where, Q represents the error weighting matrix, $Q = \text{diag}(q_1, q_2, \cdots, q_P)$, while R denotes the control weighting matrix $R = \text{diag}(r_1, r_2, \cdots, r_M)$.

The control quantity, aimed to be optimized in subsequent M steps, is determined by minimizing this performance criterion, based on the condition for the function's minimum value:

$$\frac{\partial J}{\partial \Delta U_M(k)} = 0 \tag{9}$$

Integrating Eqs. (7), (8), and (9), the formulation for the control increment matrix $\Delta U_M(k)$ is obtained:

$$\Delta U_M(k) = \left(A^T Q A + R\right)^{-1} A^T Q \times [U_{ref}(k) - U_{P0}(k)] \tag{10}$$

The optimization matrix, denoted as $\mathrm{g}^T = A^T(QA + R)^{-1}A^T Q$, facilitates the calculation of the control increment matrix $\Delta U_M(k)$ at moment k through g^T. The control quantity $u_{\mathrm{c}}(k)$ at moment k is then ascertained by adding the foremost element $\Delta u_{\mathrm{c}}(k)$ of the control increment matrix to the control quantity $u_{\mathrm{c}}(k-1)$ of the preceding moment:

$$u_{\mathrm{c}}(k) = u_{\mathrm{c}}(k-1) + \Delta u_{\mathrm{c}}(k) \tag{11}$$

This process highlights that the optimization control procedure within DMC is an ongoing, online activity. Post-implementation of the control quantity $u_{\mathrm{c}}(k-1)$ at moment $k-1$, optimization at the subsequent moment k is conducted and cumulatively added to the current value $\Delta u_{\mathrm{c}}(k)$. Typically, the error weighting matrix Q is an identity matrix, q_i=1, and the control weighting matrix R, aimed at restraining excessive control increments, is chosen as a zero matrix, r_i=0. With these parameters P, M, Q, R, and established, g^T can be directly computed, thereby reducing the real-time computational burden and streamlining the control law computation.

2.3.3 Error feedback correction

During the rolling optimization phase within the DMC framework, the summation of control increments $\Delta u_{\mathrm{c}}(k)$ at moment k is equated to introducing a step change in amplitude $\Delta u_{\mathrm{c}}(k)$ at the input. Consequently, the predicted output voltage for ensuing N moments is computed as per Eq. (12):

$$U_{N1}(k) = U_{N0}(k) + \boldsymbol{u}\Delta u_{\mathrm{c}}(k) \tag{12}$$

where,

$$U_{N1}(k) = \begin{bmatrix} U_{N1}(k+1|k) & U_{N1}(k+2|k) & \cdots & U_{N1}(k+N|k) \end{bmatrix}^T$$

$$U_{N0}(k) = \begin{bmatrix} U_{N0}(k+1|k) & U_{N0}(k+2|k) & \cdots & U_{N0}(k+N|k) \end{bmatrix}^T$$

where, $U_{N1}(k)$ signifies the matrix of predicted voltage values at future N moments, influenced by the control increment $\Delta u_{\mathrm{c}}(k)$ at moment k. $U_{N0}(k)$ stands as the matrix of initial predicted voltage values for future N moments starting from moment k.

In real-world scenarios, factors such as environmental disturbances and model mismatches can lead to variances between predicted and actual output values post-optimization. To rectify this, error feedback is integrated for parameter correction, facilitating precise and prompt tracking of the output voltage. Using moment k as the reference point, the predicted value $U_{N1}(k+1|k)$ at moment $k+1$, and the actual sampled value $U(k+1)$ at the same moment are compared. This comparison yields the output error:

$$e(k+1) = U(k+1) - U_{N1}(k+1 \mid k) \tag{13}$$

The DMC algorithm employs an error-weighted approach to amend future output predictions, thus recalibrating the predicted voltage $U_{\text{cor}}(k+1)$:

$$U_{cor}(k+1) = U_{N1}(k) + \boldsymbol{h}e(k+1) \tag{14}$$

where,

$$U_{\text{cor}}(k+1) = \begin{bmatrix} U_{\text{cor}}(k+1) & U_{\text{cor}}(k+2) & \cdots & U_{\text{cor}}(k+N) \end{bmatrix}^T$$

h is the error correction vector, and h=$\begin{bmatrix} h_1 & h_2 & \cdots & h_N \end{bmatrix}^T$, typically with the correction coefficient h_1=1 set at a predefined value.

As the process progresses, the focus shifts from moment k to moment $k+1$, with this transition being represented by the shift matrix.

$$S = \begin{bmatrix} 0 & 1 & \cdots & 0 \\ \vdots & \vdots & \vdots & \vdots \\ \vdots & \vdots & 0 & 1 \\ 0 & 0 & \cdots & 1 \end{bmatrix}$$

Applying this matrix to the revised predicted voltage facilitates the establishment of the initial voltage prediction for moment $k+1$:

$$U_{N0}(k+1) = SU_{cor}(k+1) \tag{15}$$

Subsequently, the foremost P elements of $U_{N0}(k+1)$ are selected as the initial predicted voltage values for the next P moments. The initial voltage prediction for these future moments is established as:

$$U_{P0}(k+1) = \begin{bmatrix} E_{P\times P} & 0 \end{bmatrix}_{P\times N} U_{N0}(k+1) \tag{16}$$

where, $E_{P\times P}$ is denoted as a P-dimensional identity matrix.

The control quantity $u_{\text{c}}(k)$ at moment k, as determined by Eqs. (10) and (11), is then implemented on the full-bridge LLC resonant converter. Concurrently, by applying Eqs. (12), (13), (14), (15), and (16), a comprehensive sequence of prediction, feedback, correction, and shifting is executed, resulting in a P-dimensional vector of predicted output voltage values. This vector is subsequently integrated into Eq. (10), perpetuating the rolling optimization process.

3 Experiments

The experimental phase was initiated to assess the feasibility and effectiveness of the DMC algorithm. For this purpose, a full-bridge LLC resonant converter model was developed utilizing Simulink software. Comparative analyses focused on the dynamic performance of systems operating under traditional PI control and DMC. Key parameters of the full-bridge LLC resonant converter and the voltage DMC controller developed for this research are detailed in Table 1 and Table 2, respectively.

System stability was defined as output voltage fluctuations remaining within 100mV under sudden load changes. Voltage response curves for both control strategies were illustrated in Figure 6. At 0.4 seconds, with an abrupt decrease in load resistance from 300Ω to 64Ω, the maximum voltage drop under traditional PI control was noted as 4.16V, and the dynamic response time was recorded at 20ms. Conversely, under DMC implementation, the maximum voltage drop was reduced to 3.76V, and the system attained a new steady state in 13ms. At 0.45 seconds, when the load resistance increased suddenly from 64Ω to 300Ω, traditional PI control yielded a maximum overshoot of 4.12V and a dynamic response time of 132ms. With DMC control, the maximum overshoot was limited to 3.48V, and the system stabilized in 125ms.

Table 1. Parameters of the full-bridge LLC resonant converter

Parameter	Value
Input voltage *Vin*/V	500
Output voltage Uo/V	400
Output capacitance Co/uF	2200
Resonant capacitance Cr/uF	1.384
Resonant inductance *Lr*/uH	29.28
Excitation inductance *Lm*/uH	175.7
Transformer turn ratio n	1.25

Table 2. DMC controller parameters

Parameter	Value
Modeling time domain N	20
Optimization time domain P	4
Control time domain M	2
Error weighting matrix Q	E
Control weighting matrix R	0
Correction vector h	$\mathrm{h1} = 1, \mathrm{hi} = 0.8(i > 1)$

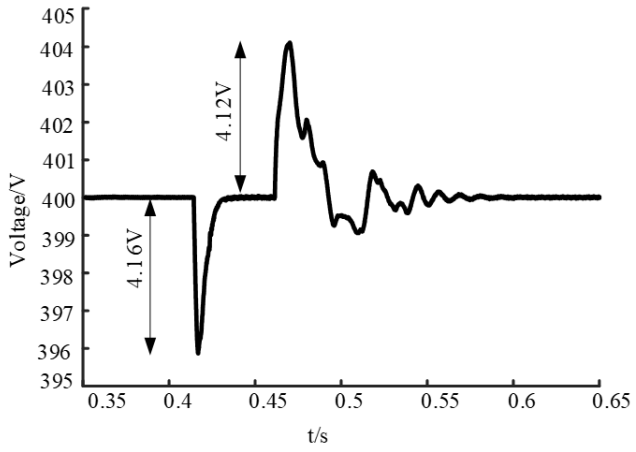

(a) PI control

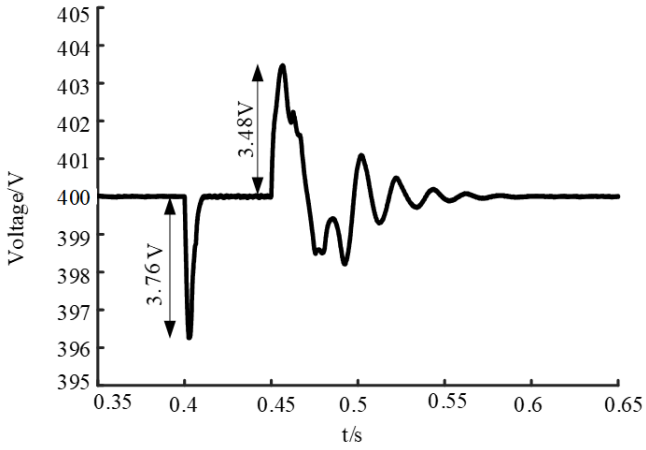

(b) DMC control

Figure 6. Output voltage response curves with sudden load changes under different control strategies

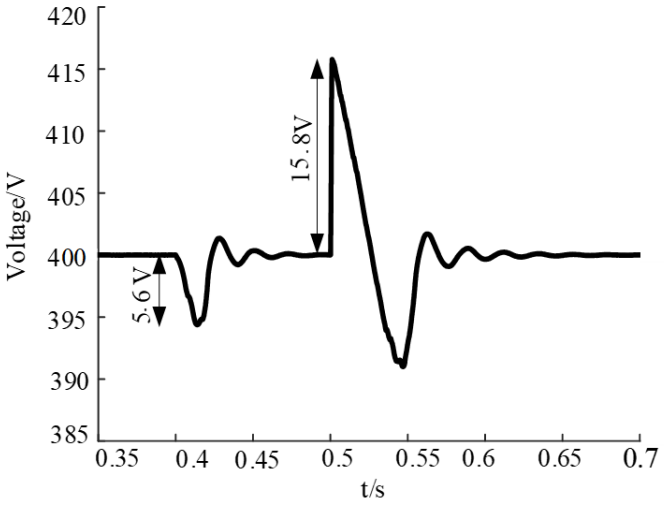

(a) PI control

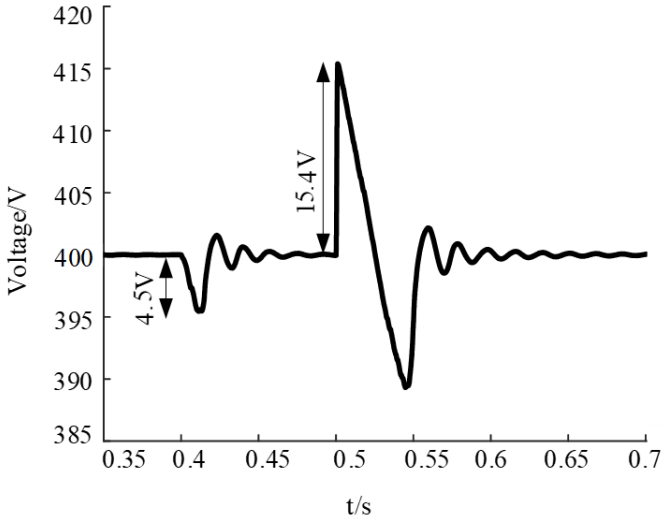

(b) DMC control

Figure 7. Output voltage response curves with sudden input voltage changes under different control strategies

In the second-phase experimental analysis, the impact of abrupt changes in system input voltage on output stability was scrutinized. Output stability was defined as voltage fluctuations remaining within a 100mV threshold. Voltage response curves, corresponding to both control strategies, are illustrated in Figure 7. At the 0.4-second mark, following a sudden decline in input voltage from 500V to 480V, the maximum voltage drop observed under traditional PI control was recorded at 5.6V, with the system's dynamic response time being 62ms. In contrast, under DMC control, the maximum voltage drop was limited to 4.5V, and the system achieved a new steady state within 60ms. Subsequently, at 0.5 seconds, when the input voltage increased sharply from 480V to 500V, the maximum overshoot with traditional PI control reached 15.8V, and the dynamic response time extended to 130ms. Conversely, with DMC control, the maximum overshoot was contained at 15.4V, and system stabilization was accomplished in 128ms.

The comparative evaluation of output voltage response curves under various control strategies during input voltage and load fluctuations clearly demonstrates that systems employing the DMC control strategy significantly outperform those using traditional PI control in terms of overshoot and dynamic response. This outcome underscores the efficacy of the DMC control strategy in managing full-bridge LLC resonant converters, thereby highlighting its potential for widespread application and its considerable practical significance.

4 Conclusions

In this study, the complexities inherent in the full-bridge LLC resonant converter model, which traditionally resulted in suboptimal control performance, have been addressed. Due to the complexity of the full-bridge LLC

resonant converter model, the control performance of the converter system is poor. Under the traditional PI control strategy, the system has problems such as slow dynamic response and large overshoot. The application of the DMC algorithm to the full-bridge LLC resonant converter, accompanied by the development of a corresponding voltage closed-loop controller, marks a significant advancement. This algorithm does not demand high precision in model parameters and has the advantages of flexible control and strong anti-interference ability. The simulation verification results showed that its control performance was better than that of the traditional PI control. In cases of sudden changes in system load and input voltage, the system using DMC control algorithm has smaller overshoot and better dynamic performance. The DMC algorithm involves comprehensive matrix calculations and high computational complexity. Moreover, its parameter adjustment requires certain professional knowledge and experience. Therefore, future research endeavors will concentrate on enhancing the performance and adaptability of the DMC algorithm, aiming to better meet the practical demands of industrial applications.

Data Availability

The data used to support the findings of this study are available from the corresponding author upon request.

Conflicts of Interest

The authors declare that they have no conflicts of interest.

References

[1] A. G. Olabi, T. Wilberforce, and M. A. Abdelkareem, "Fuel cell application in the automotive industry and future perspective," *Energy*, vol. 214, p. 118955, 2021. https://doi.org/10.1016/j.energy.2020.118955

[2] A. Giampieri, J. Ling-Chin, Z. Ma, A. Smallbone, and A. P. Roskilly, "A review of the current automotive manufacturing practice from an energy perspective," *Appl. Energy*, vol. 261, p. 114074, 2020. https://doi.org/10.1016/j.apenergy.2019.114074

[3] D. Ravi, B. M. Reddy, S. L. Shimi, and P. Samuel, "Bidirectional DC to DC converters: An overview of various topologies, switching schemes and control techniques," *Int. J. Eng. Technol.*, vol. 7, no. 4.5, pp. 360–365, 2018.

[4] Y. Wei, Q. Luo, and A. Mantooth, "A hybrid half-bridge LLC resonant converter and phase shifted full-bridge converter for high step-up application," in *2020 IEEE Workshop on Wide Bandgap Power Devices and Applications in Asia (WiPDA Asia), Suita, Japan*, 2020, pp. 1–6. https://doi.org/10.1109/WiPDAAsia49671.2020.9360292

[5] S. T. Wu and C. H. Han, "Design and implementation of a full-bridge LLC converter with wireless power transfer for dual mode output load," *IEEE Access*, vol. 9, pp. 120 392–120 406, 2021. https://doi.org/10.1109/ACCESS.2021.3107868

[6] P. Rehlaender, F. Schafmeister, and J. Boecker, "Interleaved single-stage LLC converter design utilizing half-and full-bridge configurations for wide voltage transfer ratio applications," *IEEE Trans. Power Electron.*, vol. 36, no. 9, pp. 10 065–10 080, 2021. https://doi.org/10.1109/TPEL.2021.3067843

[7] Z. Li, Y. Wei, S. Zhang, and J. Liu, "A simple optimal trajectory and thermal balance control strategy for full-bridge LLC resonant converter with wide voltage range application," *IEEE Trans. Power Electron.*, 2023. https://doi.org/10.1109/TPEL.2023.3336634

[8] L. Ma, X. Cao, R. Fu, T. Zhou, and Z. Shu, "Transient response improvement of half-bridge LLC resonant converter with full-bridge rectifier for DC microgrid," *IET Renew. Power Gen.*, 2023. https://doi.org/10.1049/rpg2.12878

[9] Y. Chen and Y.-F. Liu, "Latest advances of LLC converters in high current, fast dynamic response, and wide voltage range applications," *CPSS Trans. Power Electron. Appl.*, vol. 2, no. 1, pp. 59–67, 2017. https://doi.org/10.24295/CPSSTPEA.2017.00007

[10] M. F. Menke, A. R. Seidel, and R. V. Tambara, "LLC LED driver small-signal modeling and digital control design for active ripple compensation," *IEEE Trans. Ind. Electron.*, vol. 66, no. 1, pp. 387–396, 2018. https://doi.org/10.1109/TIE.2018.2829683

[11] Z. Fang, J. Wang, S. Duan, K. Liu, and T. Cai, "Control of an LLC resonant converter using load feedback linearization," *IEEE Trans. Power Electron.*, vol. 33, no. 1, pp. 887–898, 2017. https://doi.org/10.1109/TPEL.2017.2672731

[12] S. W. Kang and B. H. Cho, "Digitally implemented charge control for LLC resonant converters," *IEEE Trans. Ind. Electron.*, vol. 64, no. 8, pp. 6159–6168, 2017. https://doi.org/10.1109/TIE.2017.2682801

[13] R. Pandey and B. Singh, "A power-factor-corrected LLC resonant converter for electric vehicle charger using cuk converter," *IEEE Trans. Ind. Appl.*, vol. 55, no. 6, pp. 6278–6286, 2019. https://doi.org/10.1109/PEDES.2018.8707550

[14] J. Zeng, G. Zhang, S. S. Yu, B. Zhang, and Y. Zhang, "LLC resonant converter topologies and industrial applications—A review," *Chin. J. Electr. Eng.*, vol. 6, no. 3, pp. 73–84, 2020. https://doi.org/10.23919/CJEE.2020.000021

[15] K. W. Kim, Y. Jeong, J. S. Kim, and G. W. Moon, "Low common-mode noise full-bridge LLC resonant converter with balanced resonant tank," *IEEE Trans. Power Electron.*, vol. 36, no. 4, pp. 4105–4115, 2020. https://doi.org/10.1109/TPEL.2020.3025576

[16] L. Shi, B. Liu, and S. Duan, "Burst-mode and phase-shift hybrid control method of LLC converters for wide output range applications," *IEEE Trans. Ind. Electron.*, vol. 67, no. 2, pp. 1013–1023, 2019. https://doi.org/10.1109/TIE.2019.2898578

[17] H. Wu, X. Zhan, and Y. Xing, "Interleaved LLC resonant converter with hybrid rectifier and variable-frequency plus phase-shift control for wide output voltage range applications," *IEEE Trans. Power Electron.*, vol. 32, no. 6, pp. 4246–4257, 2017. https://doi.org/10.1109/TPEL.2016.2602545

[18] H. Wang and Z. Li, "A PWM LLC type resonant converter adapted to wide output range in PEV charging applications," *IEEE Trans. Power Electron.*, vol. 33, no. 5, pp. 3791–3801, 2017. http://doi.org/10.1109/TPEL.2017.2713815

[19] G. Li, D. Yang, B. Zhou, Y. F. Liu, and H. Zhang, "Integration of three-phase LLC resonant converter and full-bridge converter for hybrid modulated multioutput topology," *IEEE J. Emerg. Sel. Topics Power Electron.*, vol. 10, no. 5, pp. 5844–5856, 2021. https://doi.org/10.1109/JESTPE.2021.3139905

[20] T. Zhu, F. Zhuo, F. Zhao, F. Wang, H. Yi, and T. Zhao, "Optimization of extended phase-shift control for full-bridge CLLC resonant converter with improved light-load efficiency," *IEEE Trans. Power Electron.*, vol. 35, no. 10, pp. 11 129–11 142, 2020. https://doi.org/10.1109/TPEL.2020.2978419

[21] Y. Wei, Q. Luo, X. Du, N. Altin, A. Nasiri, and J. M. Alonso, "A dual half-bridge LLC resonant converter with magnetic control for battery charger application," *IEEE Trans. Power Electron.*, vol. 35, no. 2, pp. 2196–2207, 2019. https://doi.org/10.1109/TPEL.2019.2922991

[22] Z. Shi, Y. Tang, Y. Guo, X. Li, and H. Sun, "Optimal design method of LLC half-bridge resonant converter considering backflow power analysis," *IEEE Trans. Ind. Electron.*, vol. 69, no. 4, pp. 3599–3608, 2021. https://doi.org/10.1109/TIE.2021.3076706